Hindawi
International Journal of Chemical Engineering
Volume 2024, Article ID 5321249, 19 pages
https://doi.org/10.1155/2024/5321249

Research Article

Numerical Integration of Some Arbitrary Functions over an Ellipsoid by Discretizing into Hexahedral Elements for Biomaterial Studies

T. M. Mamatha,[1] B. Venkatesh,[1] P. Senthil Kumar,[2] S. Mullai Venthan,[1] M. S. Nisha,[3] and Gayathri Rangasamy[4,5]

[1]*Department of Mathematics, Amrita School of Engineering, Amrita Vishwa Vidyapeetham, Bengaluru, India*
[2]*Centre for Pollution Control and Environmental Engineering, Pondicherry University, School of Engineering and Technology, Kalapet, Puducherry 605014, India*
[3]*School of Aeronautical Sciences, Hindustan Institute of Science and Technology, Chennai, India*
[4]*Department of Sustainable Engineering, Institute of Biotechnology, Saveetha School of Engineering, SIMATS, Chennai 602105, India*
[5]*School of Engineering, Lebanese American University, Byblos, Lebanon*

Correspondence should be addressed to B. Venkatesh; b_venkatesh@blr.amrita.edu and P. Senthil Kumar; senthilkumarp@pondiuni.ac.in

Received 9 November 2023; Revised 14 January 2024; Accepted 2 February 2024; Published 19 February 2024

Academic Editor: Jitendra Kumar

This study mathematically examines chemical and biomaterial models by employing the finite element method. Unshaped biomaterials' complex structures have been numerically analyzed using Gaussian quadrature rules. It has been analyzed for commercial benefits of chemical engineering and biomaterials as well as biorefinery fields. For the computational work, the ellipsoid has been taken as a model, and it has been transformed by subdividing it into six tetrahedral elements with one curved face. Each curved tetrahedral element is considered a quadratic and cubic tetrahedral element and transformed into standard tetrahedral elements with straight faces. Each standard tetrahedral element is further decomposed into four hexahedral elements. Numerical tests are presented that verify the derived transformations and the quadrature rules. Convergence studies are performed for the integration of rational, weakly singular, and trigonometric test functions over an ellipsoid by using Gaussian quadrature rules and compared with the generalized Gaussian quadrature rules. The new transformations are derived to compute numerical integration over curved tetrahedral elements for all tests, and it has been observed that the integral outcomes converge to accurate values with lower computation duration.

1. Introduction

Three-dimensional volume integrals have an extensive variety of implementations in science and engineering. Calculation of certain functions over the ellipsoid surface remains extremely significant in electromagnetic theory, shell structures, cartography, geodesics, and numerous manufacturing problems. In physical science, the calculation of framework, the moment of inertia, and force upon a 3D entity involve triple integrals' evaluation. Surface integrals are utilized as a part of different zones of material science and designing for issues including computations of the frame of a shell, mass's focal point, snapshots of shell's inactivity, liquid stream as well as a mass stream over a surface, electric charge dispersed across a surface, plate twisting, plane strain, warm conduction across a plate, and comparative issues within a building's different territories that remain extremely hard to break down utilizing logical systems. The finite element method (FEM) has to turn out to be a great implementation for the mathematical solution of

a large number of manufacturing problems, especially if analytics solutions remain unavailable or extremely arduous to achieve the outcomes. An actual technique to execute large-scale simulations is to use advanced finite elements that remain renowned for convergence's quicker rate concerning computative efficacy. The finite elements in 3D curved domains should be perfectly curved for preserving the convergence speed while implementing high-order FEM. Arithmetic methodologies for integration asses the provided function's definitive integral by function values' weighted total at specific points. There remain several quadrature methodologies present to approximate numerical integrals. As of the literature survey, we can understand few workings in numerical integration utilizing Gaussian quadrature over the different areas [1–4]. The surface area's assessment of an ellipsoid and related integrals has been presented in [5–7]. Generalized Gaussian quadrature nodes and weights for a few polynomial and logarithmic functions are specified in [8]. In [9], the authors presented a generalized quadrature method to solve double integrals of some integrands over an elliptical region. Curved elements are generally utilized as a part of the setting of finite element techniques. The technique discovered by Zlámal [10, 11] is perceived as a principal finite element technique for a precise boundary portrayal. Triangular elements (1-curved side) have been presented with the isoparametric transformations altered to transform a reference element into the triangular element using a precise boundary elucidation. A related method has been introduced by Scott [12] by employing triangular elements having a 1-curved edge conforming to the precise boundary. Contrasting options to the typical polynomial estimate of arrangements are likewise proposed inside the setting of curved finite elements having a precise boundary portrayal, for example, the logical basis by Wachspress [13]. In any case, all these FEMs having precise boundary portrayal do not remain reasonable devices, yet rather a scientific glorification, because of the difficulty to stretch out the plans to three-dimensional (3D) areas. Gordon and Hall [14, 15] portrayed an inflection point in conventional methodology's advancement to precisely consider curved limits by using transfinite elements. The fundamental conception remained using blending functions for establishing a mapping betwixt a reference square and a subdomain having four parametric curves defining the boundary. Nonetheless, Gordon–Hall-type mappings experience the ill effects of two disadvantages, which are experienced in 3D issues. To begin with, the transformations are not generally bijective and, sometimes, prompt particular Jacobian matrices as in [16]. Furthermore, the formulations of these transformations might involve nonpolynomial functions and are exceedingly difficult in three dimensions. To evaluate the volume and boundary integrals, higher-order integration algorithms must be applied. However, higher-order quadrature rules for tetrahedral remain difficult to implement as well as computably costly turning assembling a time-consuming process. Linear tetrahedral elements concede just homogeneous misshaping and are surely understood for their solid conduct and volumetric locking; subsequently, quadratic tetrahedral elements have awesome significance in the field. Additionally, straight-sided (straight edges and level faces) elements are portrayed by steady metric to be the specific Jacobian determinant of a worldwide neighborhood organization that is free of regular directions; subsequently, explanatory reconciliation result is straightforward and simple to actualize appearances. A Jacobian framework is direct for a curved-edged component, and the metric for coordinates is cubic. Analytical integration yields an accurate mass framework, which is used as a reference esteem in advanced numerical analysis to calculate inaccuracy in other numerical schemes. Using parametric representations to turn a conventional tetrahedron into conventional one-cube elements, Rathod and Venkatesh [4] established Gauss–Legendre quadrature procedures to evaluate arbitrary integrands upon the p^3 tetrahedral elements. The volume of the standard tetrahedral element V_i discretized as p^3 tetrahedral element is $1/6p^3$ units. Mamatha and Venkatesh [17] have presented Gauss–Legendre quadrature rules for the calculation of triple integrals of some arbitrary integrands on a standard tetrahedron $T(0, 1)$: discretizing the standard tetrahedron to 4 hexahedral elements $H(-1, 1)$. The authors showed that integral results can be converged into accurate solutions with the fewest tetrahedral divisions; the total computational cost and errors are significantly decreased. They evaluated values of triple integrals of some integrands over a standard tetrahedron using generalized Gaussian quadrature rules as in [18, 19]. In [20], the higher-order cubature rules are derived over tetrahedron and tested over some sample functions for verifying the results. In [21], high-order numerical quadrature in a tetrahedron is derived with an implicitly curved interface. The efficiency of hexahedral element over tetrahedral is given by [22], and the authors examine the influence of numerical integration on finite element methods using quadrilateral or hexahedral meshes in the time domain. A special attention is provided to the use of Gauss–Lobatto points to perform mass lumping for any element order and also provided some theoretical results through several error estimates that are completed by various numerical experiments.

The evaluation of a product's moisture content and temperature experiencing low-pressure superheated steam drying has been carried out in [23]. It has been proposed with simple liquid diffusion's employment, which is a 3D model. In the modeling research, the heat and mass transfer behavior has been analyzed for the biomaterial model. Further, for illustrating deterioration bounded by surface eroding scenarios, the theoretical minimal size matrix has been modeled in [24], and it has been computed for diverse kinds of polymers and, later, validated by the available data out of the literature. An added category of expressions attributes dissolution- and/or deterioration-related release that remains reliant on the matrix's hydration and polymer's erosion. In [25], the theoretical approach has been made to biomaterials and biological structures to evaluate the physical and mechanical properties. It has been analyzed in two different ways, such as analytical and experimental. It shows the effective results and validations between the solving procedures. The properties of Poisson's ratio, yield

stress, and elastic modulus for additive manufacturing porous biomaterials have been scrutinized in [26]. It has been analyzed numerically and analytically by reiterating a similar octahedral unit cell in entire spatial trajectories. From [27], biomaterial's deformation processes are mathematically modeled and analyzed. In addition, a rheological model of 2D viscoelastic biomaterial has been modeled and described with fractional order; then, biomaterial's heat and mass transfer procedure has been also investigated. The computational results of biomaterials' heat and mass transfer procedures have been regarded considering the fractal framework. In [28], a computational paradigm of magnesium biodegradation's chemistry has been evolved and applied in a three-dimensional paradigm. It has been substantiated by correlating the anticipated and experientially acquired pH modification in saline and buffered solutions. This mathematical model remains valid to use for practical cases.

In the presented research work, the structures of the biomaterial have been analyzed mathematically. The novelty of the study is the numerical study that has been carried out to analyze the structural properties of biomaterials and biorefineries. It has transformed an ellipsoid into a unit sphere and discretized the sphere (first octant region) into six tetrahedral elements (each element is 10-noded with one curved face). Each curved tetrahedral element can be transformed into a standard tetrahedral element with straight sides; later, each standard tetrahedron is decomposed into four hexahedral elements. The values of triple integrals of certain integrands over the ellipsoid are calculated with the defined discretization to analyze the convergence rate and computational time of the integrands by using numerical integration methods. Gaussian quadrature rules have been used, which are derived as in [17], to evaluate numerical integral values over ellipsoid by discretizing conventional tetrahedron into 4 hexahedral elements and to compare the results with the generalized Gaussian quadrature rules as in [19]. Subject to these literature studies, the applications and the future scope of the present study have been modeled and discussed as follows.

2. Applications of the Study

The computational pipeline that includes the acquisition of experimental data or images, mathematical modeling, geometric modeling, material modeling, arithmetic estimation, visualization, and authentication is a well-established pipeline and is often used in biomedical computing applications. Therefore, for the numerical approximation and visualization methods, it becomes necessary for making a separate paradigm geometry's decay into a "mesh." Input for computational simulation and geometric foundation for various visualization outputs are served by these generated meshes in recent times compared to the past where the efforts to effectively produce biomedical simulations that were used to comprehend, plan, and diagnose biomedical disorders were hampered by the production of these meshes.

The tetrahedral process's initial stage remains the extraction of edge surfaces betwixt various segmentations. The first method that is frequently applied in numerous methods for extracting boundaries from the segmented data is to utilize a surfacing algorithm, like Marching Cubes. In this method, a triangle meshes series that represent the borders betwixt the features in the volumetric data is produced.

The space partition property is frequently disregarded by the Marching Cube algorithms though they produce smoother models, and, subsequently by every other subvolume, the call for each subvolume is completely encapsulated. Consequently, in order to adhere to the Marching Cubes algorithms' needs, the segmentations should be in constant and frequent change. The other option is to emit a quadrilateral face with a distinct segmentation value between any two voxels. A segmentation boundary stairstep model with several interesting qualities is thus yielded, and the newly yielded geometry has zero gaps with entire edges shut, and each shut portion has a category. When the triangular mesh defining these boundaries has been created and the boundaries from the volumetric data have been generated, the next phase comes into place. In this phase in the workflow, mesh optimization upon the boundary for maximizing mesh quality and imposition of limitations on the nodes' placement are carried out. The pipeline with several tools is provided to help boundary optimization that occurs due to the various constraints that must be adhered to by the generated mesh.

In addition to geometric and mesh oathing methods, the tools also incorporate surface remeshing algorithms and mesh topology modifiers. In the following part, these algorithms will be covered in more detail. The last phases within the pipeline involve creating a tetrahedralization or another volumetric mesh making sure that it would remain appropriate for the ensuing assessment when a proper boundary mesh has been built. Currently, there are techniques for volumetric smoothing, mesh refinement, and tetrahedral mesh generation in the SCIRun pipeline. To verify that the meshes created have sufficient quality components for computative assessment, the last phase remains in applying mesh authentication tools.

SCIRun has functionality for processing hexahedral elements directly alongside the tetrahedralization pipeline. Hexahedral meshes having stair-stepped boundaries and hexahedral meshes having smooth boundaries are the two main approaches used in SCIRun for hexahedral meshes. The resolution of these meshes is often more than needed or desired because the hexahedral meshes can be generated directly from the segmented model 6 Callahan, Cole, Shepherd, Stinstra, and Johnson. As a result, data reduction is frequently required. To resample the data at coarser hexahedral portrayals, SCIRun has algorithms. Resampling can also be used to create a coarse lattice, along with some localized refinement approaches for recovering data in crucial regions back to the original data's level or levels higher than that, which is occasionally required for specific simulations and is limited by criteria apart from the volumetric data. The hexahedral workflow is completed using volumetric smoothing and refinement approaches ensued by

mesh authentication to make sure the consequential mesh remains appropriate for further study.

For many physical applications, especially for second-order hyperbolic models, i.e., of the form

$$\frac{\partial^2 u}{\partial t^2} + \mathrm{Au} = 0, \tag{1}$$

where A denotes some positive symmetric second-order differential operator, used for the simulation of linear wave propagation phenomena. Example of its application includes the 2D acoustic wave equation, the 3D linear elasticity system, the Maxwell's equation, a poro-elasticity model, and the Reissner–Mindlin plate model. The computation of the stiffness matrix, induced by the operator A, requires the use of the quadrature formula. When general hexahedral matrices (isoparametric elements) are used, the stiffness matrix's entries cannot be computed analytically and the finite element space's basis functions are no longer locally polynomial.. Thus, an affine map is employed for analysis to transform the current element from the reference element.. When dealing with isoparametric elements, rational functions in each element's approximation space are employed .

3. Mathematical Modelling

3.1. Transformation of an Ellipsoid into Standard Arbitrary Tetrahedrons with Straight Sides for Computation of 3D Integrals. Three-dimensional volume integrals have wide-ranging applications in engineering sciences, and evaluation of the triple integrals of certain functions over ellipsoid and ellipsoid surfaces is a significant problem popular in electromagnetic theory, shell structures, cartography, geodesics, and various manufacturing problems.

The physical meaning of some parameters in the examples of the paper is E-ellipsoid, S-sphere, T-curved tetrahedral element, $\widehat{T}$-standard tetrahedral element, H-hexahedral elements, (x_I^*, y_I^*, z_I^*)-nodal coordinates for curved tetrahedra, (r, s, t)-nodal coordinates for standard tetrahedra, (ξ, η, μ)-nodal coordinates for hexahedra, J-Jacobian for transformation, and w-weight coefficients.

Consider an ellipsoid (E)

$$\frac{X^2}{a^2} + \frac{Y^2}{b^2} + \frac{Z^2}{c^2} = 1. \tag{2}$$

We transform the ellipsoid into a unit sphere as in Figure 1 using the transformation-1

$$x = \frac{X}{a}, \quad y = \frac{Y}{b}, \quad z = \frac{Z}{c}, \tag{3}$$

and the Jacobian of the transformation-1 is

$$\begin{aligned} |J_1| &= \frac{\partial(X, Y, Z)}{\partial(x, y, z)} \\ &= \begin{vmatrix} \frac{\partial X}{\partial x} & \frac{\partial X}{\partial y} & \frac{\partial X}{\partial z} \\ \frac{\partial Y}{\partial x} & \frac{\partial Y}{\partial y} & \frac{\partial Y}{\partial z} \\ \frac{\partial Z}{\partial x} & \frac{\partial Z}{\partial y} & \frac{\partial Z}{\partial z} \end{vmatrix} \\ &= \mathrm{abc}. \end{aligned} \tag{4}$$

The triple integral evaluation on ellipsoid (E) changes to an integral evaluation on a sphere (S) of radius one as follows:

$$\begin{aligned} I &= \iiint_E f(X, Y, Z)\mathrm{d}Z\mathrm{d}Y\mathrm{d}X \\ &= \iiint_S f(\mathrm{ax}, \mathrm{by}, \mathrm{cz})|J_1|\mathrm{d}z\mathrm{d}y\mathrm{d}x \\ &= \mathrm{abc}\iiint_S g(x, y, z)\mathrm{d}z\mathrm{d}y\mathrm{d}x. \end{aligned} \tag{5}$$

3.2. A Sphere Discretized into Arbitrary 10-Noded Tetrahedral Elements and Transforming Every Tetrahedral Element into 4 Hexahedral Elements. The unit-sphere (S) region (first octant) is considered and discretized into six smaller elements by selecting point P on the sphere surface as in Figure 2. An entire sphere is discretized into 48 tetrahedral elements with one curved face. Every discretized region here represents curved tetrahedral elements with one curved face.

The disoriented curved tetrahedral elements are transformed to the standard alignment by transformation-2, as in Table 1. All the 6-curved tetrahedrons have a common Jacobian, as in

$$\begin{aligned} |J_2| &= \frac{\partial(x, y, z)}{\partial(x^*, y^*, z^*)} \\ &= \begin{vmatrix} \frac{\partial x}{\partial x^*} & \frac{\partial x}{\partial y^*} & \frac{\partial x}{\partial z^*} \\ \frac{\partial y}{\partial x^*} & \frac{\partial y}{\partial y^*} & \frac{\partial y}{\partial z^*} \\ \frac{\partial z}{\partial x^*} & \frac{\partial z}{\partial y^*} & \frac{\partial z}{\partial z^*} \end{vmatrix} \\ &= \frac{1}{\sqrt{6}}. \end{aligned} \tag{6}$$

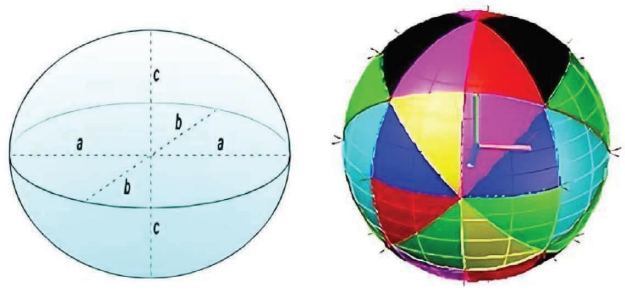

Figure 1: Transform an arbitrary ellipsoid into a sphere (radius one).

Figure 2: First octant sphere split into six tetrahedral components.

Table 1: Transformation-2.

Element	X	Y	Z
1	$x^* + y^*/\sqrt{2} + z^*/\sqrt{3}$	$y^*/\sqrt{2} + z^*/\sqrt{3}$	$z^*/\sqrt{3}$
2	$x^*/\sqrt{2} + z^*/\sqrt{3}$	$x^*/\sqrt{2} + y^* + z^*/\sqrt{3}$	$z^*/\sqrt{3}$
3	$z^*/\sqrt{3}$	$x^* + y^*/\sqrt{2} + z^*/\sqrt{3}$	$y^*/\sqrt{2} + z^*/\sqrt{3}$
4	$z^*/\sqrt{3}$	$x^*/\sqrt{2} + z^*/\sqrt{3}$	$x^* + y^*/\sqrt{2} + z^*/\sqrt{3}$
5	$y^*/\sqrt{2} + z^*/\sqrt{3}$	$z^*/\sqrt{3}$	$x^* + y^*/\sqrt{2} + z^*/\sqrt{3}$
6	$x^*/\sqrt{2} + y^* + z^*/\sqrt{3}$	$z^*/\sqrt{3}$	$x^*/\sqrt{2} + z^*/\sqrt{3}$

The triple integral over a sphere (S), as in equation (5), is transformed into a triple integral over the curved-sided standard tetrahedral element (T), as in the following equation:

$$\begin{aligned} I &= \mathrm{abc}\iiint_S g(x,y,z)\mathrm{d}z\mathrm{d}y\mathrm{d}z \\ &= \mathrm{abc}\sum_{V_{i=1}}^{6}\iiint_T G(x^*,y^*,z^*)|J_2|\mathrm{d}z^*\mathrm{d}y^*dx^* \\ &= \frac{\mathrm{abc}}{\sqrt{6}}\sum_{V_{i=1}}^{6}\iiint_T G(x^*,y^*,z^*)\mathrm{d}z^*\mathrm{d}y^*\mathrm{d}x^*. \end{aligned} \tag{7}$$

The curved tetrahedral elements are considered to be quadratic tetrahedral (10-noded) and cubic tetrahedral (20-noded) elements and transformed into straight-sided tetrahedral elements, respectively, using two different transformations as discussed below.

3.3. Arbitrary Quadratic Tetrahedral Curved Elements Transformed to Standard Straight-Sided Tetrahedral Elements. Each 10-noded curved tetrahedral element (one curved face) is transformed into standard tetrahedral elements with straight sides, as in Figure 3, using transformation-3, as in equation (8).

3.3.1. Transformation-3

$$\begin{aligned} x^* &= r + 2[2x_8^* - 1]\mathrm{rs} + 2[2x_{10}^* - 1]\mathrm{rt}, \\ y^* &= s + 2[2y_8^* - 1]\mathrm{rs} + 2[2y_9^* - 1]\mathrm{st}, \\ z^* &= t + 2[2z_9^* - 1]\mathrm{st} + 2[2z_{10}^* - 1]\mathrm{rt}. \end{aligned} \tag{8}$$

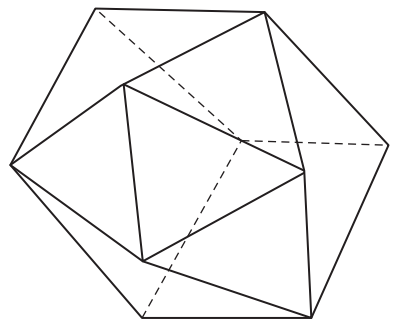

Figure 3: Standard tetrahedron elements transformed to have straight edges.

For all six elements, we get a common Jacobian, as in the following equation:

$$
\begin{aligned}
|J_3| &= \frac{\partial(x^*, y^*, z^*)}{\partial(r, s, t)} \\
&= \begin{vmatrix} \frac{\partial x^*}{\partial r} & \frac{\partial x^*}{\partial s} & \frac{\partial x^*}{\partial t} \\ \frac{\partial y^*}{\partial r} & \frac{\partial y^*}{\partial s} & \frac{\partial y^*}{\partial t} \\ \frac{\partial z^*}{\partial r} & \frac{\partial z^*}{\partial s} & \frac{\partial z^*}{\partial t} \end{vmatrix} \\
&= 1 + 0.416849395r + 0.263374889s + 0.350655496t + 0.057782553\text{rs} \\
&\quad + 0.041097389\text{st} + 0.066387592\text{rt} + 0041536378r^2 + 0.016246174s^2 \\
&\quad + 0.024851212t^2 + 0.016380368\text{rst}.
\end{aligned}
\tag{9}
$$

The triple integral over a sphere (S), as in equation (7), is transformed into a triple integral on straight-sided standard quartic tetrahedron elements (T) as in the following equation:

$$
\begin{aligned}
I &= \text{abc}\iiint_S g(x, y, z)dzdydx = \frac{\text{abc}}{\sqrt{6}}\sum_{V_{I=1}}^{6}\iiint_T G(x^*, y^*, z^*)dz^*dy^*dx^* \\
&= \frac{\text{abc}}{\sqrt{6}}\sum_{V_{i=1}}^{6}\iiint_T F(r, s, t)|J_3|drdsdt.
\end{aligned}
\tag{10}
$$

3.4. Arbitrary Cubic Tetrahedral Curved Elements Transformed to Standard Straight-Sided Tetrahedral Elements. The transformation that transforms a curved tetrahedron T into an orthogonal tetrahedron $\widehat{T}$ is as follows:

$$\begin{aligned} T &= \sum_{i=1}^{20} N_i(r,s,t)T_i, \\ T &= (x^*, y^*, z^*) \text{ and} \\ T_i &= (x_i^*, y_i^*, z_i^*), \end{aligned} \tag{11}$$

that is,

$$\begin{aligned} T(x^*, y^*, z^*) = {} & t_4 + (t_1 - t_4)r + (t_{21} - t_4)s + (t_1 - t_4)t + \frac{9}{4}(-t_1 - t_2 + t_{11} + t_{12})\mathrm{rs} \\ & + \frac{9}{4}(-t_2 - t_3 + t_{13} + t_{14})\mathrm{st} + \frac{9}{4}(-t_1 - t_3 + t_{15} + t_{16})\mathrm{rt} \\ & + \frac{9}{4}\left[2(t_1 + t_2 + t_3) - 3(t_{11} + t_{12} + t_{13} + t_{14} + t_{15} + t_{16}) + t_{20}\right]\mathrm{rst}, \end{aligned} \tag{12}$$

where $N_i(r,s,t)$ are nodal coordinates of orthogonal tetrahedron.

Nodal coordinates $(x_i^*, y_i^*, z_i^*), i = 1(1)20$ over curved tetrahedron are given as follows.

For the above nodal data from Table 2, the transformation is as in equation (13).

$$\begin{aligned} x^* &= r + 0.165487\mathrm{rs} + 0.253652\mathrm{rt} - 0.196443\mathrm{rst}, \\ y^* &= s + 0.165487\mathrm{rs} + 0.0988491\mathrm{st} + 0.267965\mathrm{rst}, \\ z^* &= t + 0.253652\mathrm{rt} + 0.0988481\mathrm{st} + 0.00347117\mathrm{rst}. \end{aligned} \tag{13}$$

For all six standard tetrahedral elements, we get a common Jacobian, as in equation (9).

3.4.1. Transformation-4

$$\begin{aligned} |J_4| &= \frac{\partial(x^*, y^*, z^*)}{\partial(r,s,t)} \\ &= \begin{vmatrix} \frac{\partial x^*}{\partial r} & \frac{\partial x^*}{\partial s} & \frac{\partial x^*}{\partial t} \\ \frac{\partial y^*}{\partial r} & \frac{\partial y^*}{\partial s} & \frac{\partial y^*}{\partial t} \\ \frac{\partial z^*}{\partial r} & \frac{\partial z^*}{\partial s} & \frac{\partial z^*}{\partial t} \end{vmatrix} \\ &= 1 + 0.352501t + 0.0250732t^2 + 0.264336s - 0.155011s - 0.0194182\mathrm{st}^2 \\ &\quad + 0.0163583s^2 - 0.0194182s^2t + 0.419139r + 0.335014r + 0.0679697\mathrm{rt}^2 + 0.0618055rs \\ &\quad + 0.0165972\mathrm{rst} + 0.00170626\mathrm{rst}^2 + 0.000574434\mathrm{rs}^2 - 0.00754011\mathrm{rs}^2t \\ &\quad + 0.0419761r^2 + 0.067969r^2t + 0.000574434r^2s + 0.0196397r^2\mathrm{st}. \end{aligned} \tag{14}$$

Table 2: Coordinates at each node for 20-nodded tetrahedral components.

I	x_i^*	y_i^*	z_i^*
1	1	0	0
2	0	1	0
3	0	0	1
4	0	0	0
5	0.3333	0	0
6	0.6666	0	0
7	0	0.3333	0
8	0	0.6666	0
9	0	0	0.3333
10	0	0	0.6666
11	0.7034	0.3701	0
12	0.3701	0.7034	0
13	0	0.6886	0.3552
14	0	0.3552	0.6886
15	0.3897	0	0.7230
16	0.7230	0	0.3897
17	0.3517	0.3517	0
18	0	0.3443	0.3443
19	0.3761	0	0.3761
20	0.3726	0.3726	0.3726

The triple integral over a sphere, as in equation (7), is transformed to a triple integral on straight-sided standard cubic tetrahedral elements as in the following equation:

$$\begin{aligned} I &= \mathrm{abc}\iiint_S g(x,y,z)\mathrm{d}z\mathrm{d}y\mathrm{d}x \\ &= \frac{\mathrm{abc}}{\sqrt{6}}\sum_{V_{I=1}}^{6}\iiint_T G(x^*,y^*,z^*)\mathrm{d}z^*\mathrm{d}y^*\mathrm{d}x^* \\ &= \frac{\mathrm{abc}}{\sqrt{6}}\sum_{V_{i=1}}^{6}\iiint_T F(r,s,t)\left|J_4\right|\mathrm{d}r\mathrm{d}s\mathrm{d}t. \end{aligned} \tag{15}$$

3.5. Standard Tetrahedron Decomposed to 4-Hexahedral Elements

3.5.1. Shape Functions. A scalar real-valued function $f(r,s,t)$ is defined over the finite volume of a standard tetrahedron. A standard tetrahedron is considered and divided into 4 hexahedrons as in Figure 4. Later, every disoriented hexahedron element is changed to a standard hexahedron element $H[-1,\ 1]^3$. Every i^{th} node (r_i, s_i, t_i) of the hexahedron volume, where the index $i = 1,\ 2,\ \ldots,\ 8$, is as shown in Figure 5. A positive volume is guaranteed by this purpose of node numbering. By transforming the Cartesian coordinates (r,s,t) to natural coordinates (ξ,η,μ) using equation (13), the limits of integration are mapped to

$$(-1 \le \xi,\eta,\mu \le 1)\ \text{in}\ (\xi,\eta,\mu)\ \text{space}\ (r,s,t) = \sum_{j=1}^{8} N_i(\xi,\eta,\mu)\left(r^j, s^j, t^j\right). \tag{16}$$

The hexahedral elements are mapped to standard orientation (2-cube elements) as shown in Figure 6.

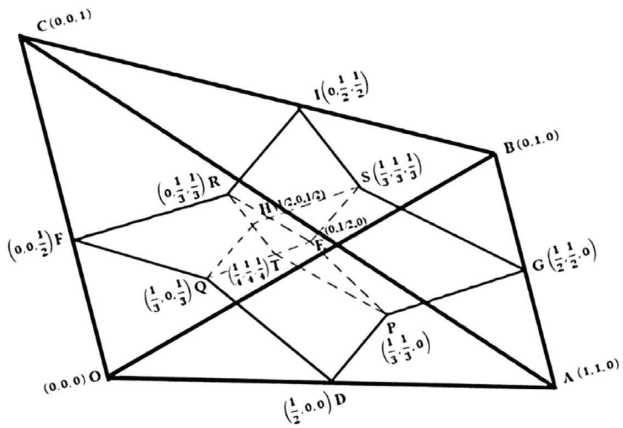

Figure 4: Four hexahedron elements from a tetrahedron.

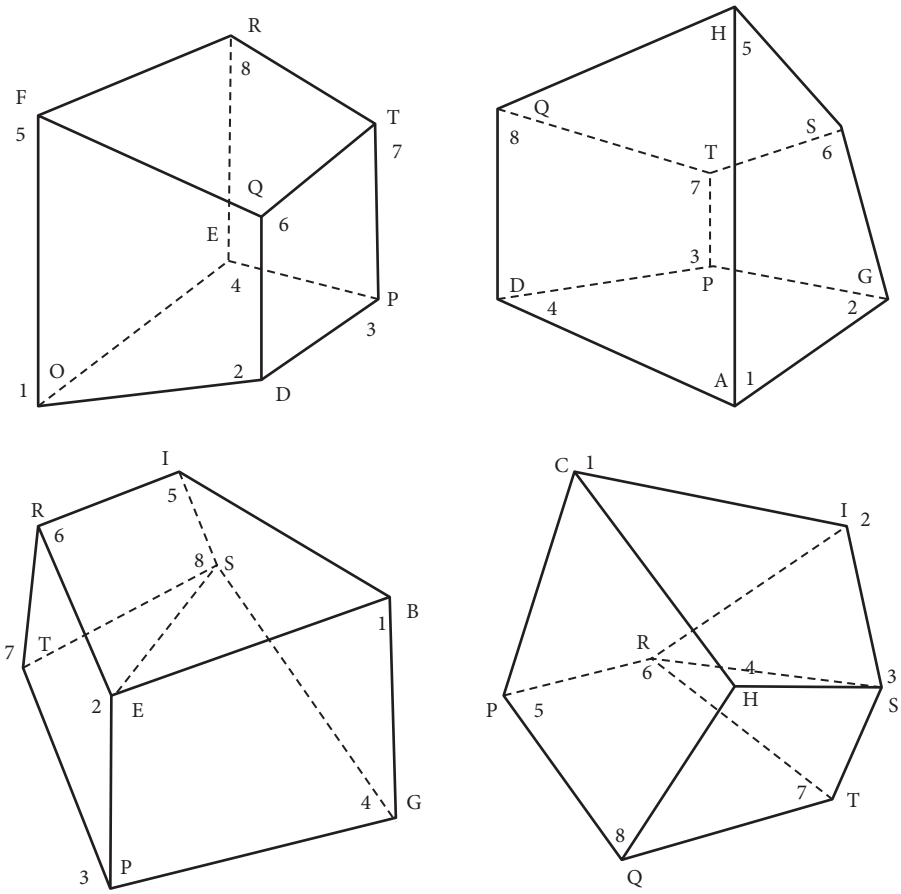

Figure 5: Hexahedral volume elements: standard for numbering nodes.

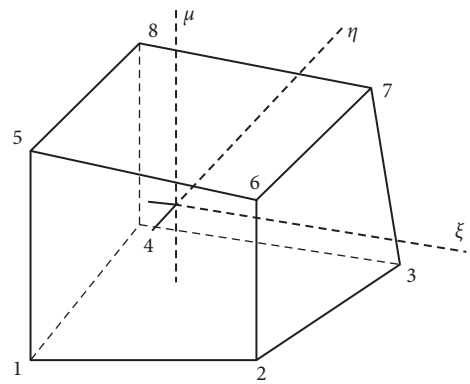

Figure 6: Cartesian coordinates of the typical hexahedral element with eight nodes.

Hexahedral elements' shape functions can be defined by

$$N_i^e(\xi,\eta,\mu) = \frac{1}{8}(1+\xi\xi_i)(1+\eta\eta_i)(1+\mu\mu_i). \tag{17}$$

The coordinates of a ith node of the resultant standard 8-node hexahedral element (H) denoted by the coordinates (ξ_i, η_i, μ_i) and the triple integral over standard tetrahedron (T), as in equations (10) and (15), can be written as

$$\begin{aligned} I &= \iiint_T F(r,s,t)\left|J_3\right| \mathrm{d}r\mathrm{d}s\mathrm{d}t \\ &= \sum_{H_{i=1}}^{4} \int_{-1}^{1}\int_{-1}^{1}\int_{-1}^{1} f(\xi,\eta,\mu)\left|J_5\right| \mathrm{d}\xi\mathrm{d}\eta\mathrm{d}\mu, \\ I &= \iiint_T F(r,s,t)\left|J_4\right| \mathrm{d}r\mathrm{d}s\mathrm{d}t \\ &= \sum_{H_{i=1}}^{4} \int_{-1}^{1}\int_{-1}^{1}\int_{-1}^{1} g(\xi,\eta,\mu)\left|J_5\right| \mathrm{d}\xi\mathrm{d}\eta\mathrm{d}\mu, \end{aligned} \tag{18}$$

where $|J_5|$ is the common Jacobian that is defined as

$$\frac{\partial(r,s,t)}{\partial(\xi,\eta,\mu)} = \begin{bmatrix} r_i\dfrac{\partial N_i^e}{\partial\xi} & s_i\dfrac{\partial N_i^e}{\partial\xi} & t_i\dfrac{\partial N_i^e}{\partial\xi} \\ r_i\dfrac{\partial N_i^e}{\partial\eta} & s_i\dfrac{\partial N_i^e}{\partial\eta} & t_i\dfrac{\partial N_i^e}{\partial\eta} \\ r_i\dfrac{\partial N_i^e}{\partial\mu} & s_i\dfrac{\partial N_i^e}{\partial\mu} & t_i\dfrac{\partial N_i^e}{\partial\mu} \end{bmatrix}. \tag{19}$$

3.5.2. Jacobian Computation for Hexahedron. The isoparametric transformation of the hexahedral elements (H) is

$$\begin{aligned} r &= r_i N_i^{(e)}, \\ s &= s_i N_i^{(e)}, \\ t &= t_i N_i^{(e)}, \end{aligned} \tag{20}$$

where $i = 1, 2, 3, \cdots, n$, n is no. of elements.

In each hexahedral element, the (r,s,t) coordinates are changed to natural coordinates (ξ,η,μ) by equation (17) as in Table 3.

$$\begin{aligned} X(\xi,\eta,\mu) &= \frac{17}{96} - \frac{\mu}{32} - \frac{\eta}{32} + \frac{\mu\eta}{96} + \frac{17\xi}{96} - \frac{\mu\xi}{32} - \frac{\eta\xi}{32} + \frac{\xi\eta\mu}{96}, \\ Y(\xi,\eta,\mu) &= \frac{17}{96} - \frac{\mu}{32} + \frac{17\eta}{96} - \frac{\mu\eta}{32} - \frac{\xi}{32} + \frac{\mu\xi}{96} - \frac{\eta\xi}{32} + \frac{\xi\eta\mu}{96}, \\ Z(\xi,\eta,\mu) &= \frac{17}{96} + \frac{17\mu}{96} - \frac{\eta}{32} - \frac{\mu\eta}{32} - \frac{\xi}{32} - \frac{\mu\xi}{32} + \frac{\eta\xi}{96} + \frac{\xi\eta\mu}{96}, \\ T(\xi,\eta,\mu) &= \frac{15}{32} - \frac{11\mu}{96} - \frac{11\eta}{96} + \frac{5\mu\eta}{96} - \frac{11\xi}{96} + \frac{5\mu\xi}{96} + \frac{5\eta\xi}{96} - \frac{\xi\eta\mu}{32}. \end{aligned} \tag{21}$$

All four hexahedral elements have a common Jacobian as in the following equation:

$$\begin{aligned} J_5 = {} & 1 + 0.350655\,\mu + 0.0248512\mu^2 + 0.263375\,\eta + 0.0410974\mu\eta + 0.0162462\eta^2 \\ & + 0.416849\xi + 0.0663876\mu\xi + 0.0577826\eta\xi + 0.0163804\xi\eta\mu + 0.0415364\xi^2. \end{aligned} \tag{22}$$

Table 3: Cartesian coordinates (x, y, z) changed to natural co-ordinates using equation (18) for all 4 hexahedral elements.

Global coordinates	Hexahedron 1	Hexahedron 2	Hexahedron 3	Hexahedron 4
r	$X(\xi,\eta,\mu)$	$T(\xi,\eta,\mu)$	$Y(\xi,\eta,\mu)$	$X(\xi,\eta,\mu)$
s	$Y(\xi,\eta,\mu)$	$X(\xi,\eta,\mu)$	$T(\xi,\eta,\mu)$	$Y(\xi,\eta,\mu)$
t	$Z(\xi,\eta,\mu)$	$Z(\xi,\eta,\mu)$	$Z(\xi,\eta,\mu)$	$T(\xi,\eta,\mu)$

We use the substitution $f(\xi,\eta,\mu) = F(r,s,t)|J_3|$ and $g(\xi,\eta,\mu) = F(r,s,t)|J_4|$ in equation (18) and use the Gauss-quadrature rule for calculating the integral

$$\begin{aligned} I &= \sum_{H_{i=1}}^{4} \int_{-1}^{1}\int_{-1}^{1}\int_{-1}^{1} f(\xi,\eta,\mu)\left|J_5\right| d\xi d\eta d\mu \\ &= \sum_{H_{i=1}}^{4} \sum_{p=1}^{n} c_p h\left(\xi_p,\eta_p,\mu_p\right), \\ I &= \sum_{H_{i=1}}^{4} \int_{-1}^{1}\int_{-1}^{1}\int_{-1}^{1} g(\xi,\eta,\mu)\left|J_5\right| d\xi d\eta d\mu \\ &= \sum_{H_{i=1}}^{4} \sum_{p=1}^{n} c_p H\left(\xi_p,\eta_p,\mu_p\right), \end{aligned} \tag{23}$$

in which n is no. of sample points, $c_p = |J_5| w_i w_j w_k$ is weight coefficients, J is Jacobian for four hexahedral elements, and (ξ_p, η_p, μ_p) is sampling points.

Transformations' efficiency derived can be exhibited by implementing the same to common cases with various sorts of integrands with some integrands chosen in such a way that exact integration is impossible because of singularity.

4. Results and Discussion

From this mathematical modeling, the structural properties of the complex and irregularly shaped biomaterials have been investigated numerically. The numerical investigation has been carried out by using the high latent method of the finite element technique. The computational results have been presented in tabular form with numerical integration examples. Moreover, the computational results have been plotted for the graphical representation of the structural properties of the biomaterials. The plotted graphical clear modeling report has been presented for the biomass and biorefinery applications.

The above-derived transformations are applied, and ensuing triple integrals on an arbitrary ellipsoid have been assessed by converting to triple integrals over quadratic tetrahedral elements and cubic tetrahedral elements. Furthermore, integrals over these elements are transformed into integrals over hexahedral elements as in equation (23). The results obtained by Gaussian quadrature rules (GQ) [17] and the generalized Gaussian quadrature rules (GGQ) are correlated to compute the integrals as tabulated in Tables 4–6. The numerical solutions of the integrands with the singularity are obtained, and the estimated outcomes remain nearer to the accurate integral values having relative errors lessened. Example functions in serial numbers 10 and 11 are considered from a research article as in [9] and are evaluated for triple integrals of the functions over an arbitrary ellipsoid by using the derived transformations. The calculated integral values are very near to the exact integral values as shown in Tables 4–6. The numerical integral values of several functions, using defined affine transformations, are tabulated as follows.

From Figures 7–14, the integrands for triple integrals with the respective functions are considered. The integral results obtained for 10-noded tetrahedron and 20-noded tetrahedron are compared by using Gaussian quadrature rules $(GQ10N, GQ20N)$ and the generalized Gaussian quadrature rules $(\mathrm{GGQ}10N, \mathrm{GGQ}20N)$. It has been observed that, when $\mathrm{GGQ}10N, \mathrm{GGQ}20N$ rules are applied for nonpolynomial functions, the exact integral values are obtained after applying $N = 10\,\&\,20$ quadrature points. Whereas $GQ10N, GQ20N$ quadrature, the outcomes remain closer to the accurate-integral values after $N = 8, 10$ quadrature points. With minimum quadrature points and the least number of decompositions, results are approaching the exact values in the proposed quadrature rules (GQ10N, GQ20N) compared to the generalized Gauss quadrature rules (GGQ10N, GGQ20N).

The structure analysis of the irregular and complex shape biomaterials has been analyzed with the Gauss quadrature rules with the same nodal points, which have been used. From Figures 7–14, for the functions that have been taken, the results get more error in the structural properties for the minimal nodal points as $\mathrm{GGQ}10N\,\&\,GQ10N$. However, when the nodal points have been increased, the errors have been reduced. Comparatively, for the nodal points $\mathrm{GGQ}20N\,\&\,GQ20N$, the results get more accurate for the complex structures of the biomaterials. For the consistent integral functions, using the finite element techniques, the errors can be reduced more rather than minimal nodal points.

Figures 15 and 16 represent the integrands for triple integrals with the functions $\sin(x^2 + y^2 + z^2)$, which has an exact value for integration, and the other function $\sin\ (x + y^2 + z^4)$, which has singularity within the domain of integration. The mentioned trigonometric integrands have not been possible to integrate analytically owing to the singularity, which lies inside the domain. Integral results have been obtained for the same nodal points 10-noded tetrahedron and 20-noded tetrahedron after discretization by moving the singular point onto the boundary of hexahedral elements. The results have been compared by using Gaussian quadrature rules $(GQ10N, GQ20N)$ and the generalized Gaussian quadrature rules $(\mathrm{GGQ}10N, \mathrm{GGQ}20N)$. It has been observed that when applied $\mathrm{GGQ}10N, \mathrm{GGQ}20N$ rules for nonpolynomial functions, the exact values are obtained after using $N = 10\,\&\,20$ quadrature points. Whereas $GQ10N, GQ20N$ quadrature, the outcomes remain closer to the accurate values after $N = 8{,}10$

Table 4: Sample functions with exact integral values.

Sl. No	Functions	Exact value
1	1	3.1416
2	$x^2 y$	0.7500
3	x^2yz	0.6914
4	$\sqrt{(x+y+z)}$	NInt = 4.6397
5	$1/\sqrt{x+y+z}$	NInt = 2.2147
6	xyz	0.7500
7	$x^2 y^2$	3.2314
8	$(1+x+y+z)^{-4}$	0.0581
9	$\sin(x+y^2+z^4)$	Singularity and highly oscillatory function
10	$\sin(x^2+y^2+z^2)$	

Table 5: Integral results for quadratic tetrahedral elements: comparison with GGQ and GQ.

Sl. No	Functions	Exact value	$10N$	GGQ ($N=5$)	$N=10$	$N=15$	$N=20$
1	$x^2 y$	2.3561	2.3632	2.3627 $N=4$ 2.3563	2.3632 $N=6$ 2.3563	2.3632 $N=8$ 2.3562	2.3632 $N=10$ 2.3561
2	1	3.1415	3.1215	3.1215 $N=4$ 3.1315	$N=6$ 3.1315	$N=8$ 3.1415	$N=10$ 3.1415
3	xyz	0.7500	0.7527481408	0.7527 $N=4$ 0.7512	$N=6$ 0.7512	$N=8$ 0.7500	$N=10$ 0.7500
4	$x^2 yz$	0.6857	0.6914	0.6914 $N=4$ 0.6884	$N=6$ 0.6860	$N=8$ 0.6859	$N=10$ 0.6857
5	$\sqrt{x+y+z}$	NInt = 4.6396	4.6108	4.6108 $N=4$ 4.6108	$N=6$ 4.6108	$N=8$ 4.6108	$N=10$ 4.6108
6	$1/\sqrt{x+y+z}$	NInt = 2.2146	2.1105	2.2008 $N=4$ 2.2005	$N=6$ 2.2007	$N=8$ 2.2008	$N=10$ 2.2008
7	$x^2 y^2$	3.2313	3.2773	3.2773 $N=4$ 3.2631	$N=6$ 3.2438	$N=8$ 3.2354	$N=10$ 3.2313
8	$(1+x+y+z)^{-4}$	0.0580	0.0419	0.04871 $N=4$ 0.0589	$N=6$ 0.0585	$N=8$ 0.0582	$N=10$ 0.0580
9	$\sin(x+y^2+z^4)$	Singularity and highly oscillatory function		1.9206 $N=4$ 1.9211	$N=6$ 1.9268	$N=8$ 9.2614	$N=10$ 9.2614
10	$\sin(x^2+y^2+z^2)$	2.2884	2.2894	2.3632 $N=4$ 2.3426	$N=6$ 2.3126	$N=8$ 2.2884	$N=10$ 2.2884
11	$x^2+y^2+z^2$	2.5132		2.4826 $N=4$ 2.4726	$N=6$ 2.4966	$N=8$ 2.5132	$N=10$ 2.5132

quadrature points. With minimum quadrature points and the least number of decompositions, results are approaching the exact values in the proposed quadrature rules compared to the generalized Gauss quadrature rules.

The structure analysis of the irregular and complex shape biomaterials has been analyzed with the Gauss quadrature rules with the same nodal points that have been used. From Figures 7–14, for the functions that have been taken, the results get more error in the structural properties for the minimal nodal points as GGQ10N & GQ10N. However, when the nodal points increase, the errors reduce. Comparatively, for the nodal points GGQ20N & GQ20N, the results get more accurate for the complex structures of the biomaterials. For the consistent integral functions, using the finite element techniques, the errors can be reduced more rather than minimal nodal points.

Table 6: Integral results of cubic tetrahedral elements: comparison with GGQ and GQ.

Sl. No	Functions	Exact value	20 N	GGQ ($N=5$)	$N=10$	$N=15$	$N=20$
1	x^2y	2.3561	2.3897	2.3627 $N=4$ 2.3563	2.3632 $N=6$ 2.3562	2.3632 $N=8$ 2.3561	2.3566 $N=10$ 2.3561
2	1	3.1415	3.1383	3.1315 $N=4$ 3.1315	$N=6$ 3.1415	$N=8$ 3.1415	$N=10$ 3.1415
3	xyz	0.7500	0.7614	0.7500 $N=4$ 0.7500	$N=6$ 0.7500	$N=8$ 0.7500	$N=10$ 0.7500
4	x^2yz	0.6857	0.6914	0.6866 $N=4$ 0.6861	$N=6$ 0.6859	$N=8$ 0.6857	$N=10$ 0.6857
5	$\sqrt{x+y+z}$	NInt = 4.6396	4.6108	4.6108 $N=4$ 4.6108	$N=6$ 4.6108	$N=8$ 4.6108	$N=10$ 4.6108
6	$1/\sqrt{x+y+z}$	NInt = 2.2146	2.2008	2.2008 $N=4$ 2.2005	$N=6$ 2.2007	$N=8$ 2.2000	$N=10$ 2.2008
7	x^2y^2	3.2313	3.2773	3.2315 $N=4$ 3.2373	$N=6$ 3.2313	$N=8$ 3.2313	$N=10$ 3.2313
8	$(1+x+y+z)^{-4}$	0.0580	0.0578	0.0581 $N=4$ 0.0583	$N=6$ 0.0580	$N=8$ 0.0580	$N=10$ 0.0580
9	$\sin(x+y^2+z^4)$	Singularity and highly oscillatory function		1.9206 $N=4$ 1.9211	$N=6$ 1.9261	$N=8$ 1.9261	$N=10$ 1.9261
10	$\sin(x^2+y^2+z^2)$	2.2884	2.2894	2.2884 $N=4$ 2.2956	$N=6$ 2.2885	$N=8$ 2.2884	$N=10$ 2.2884
11	$x^2+y^2+z^2$	2.5132		2.5132 $N=4$ 2.4987	$N=6$ 2.5138	$N=8$ 2.5132	$N=10$ 2.5132

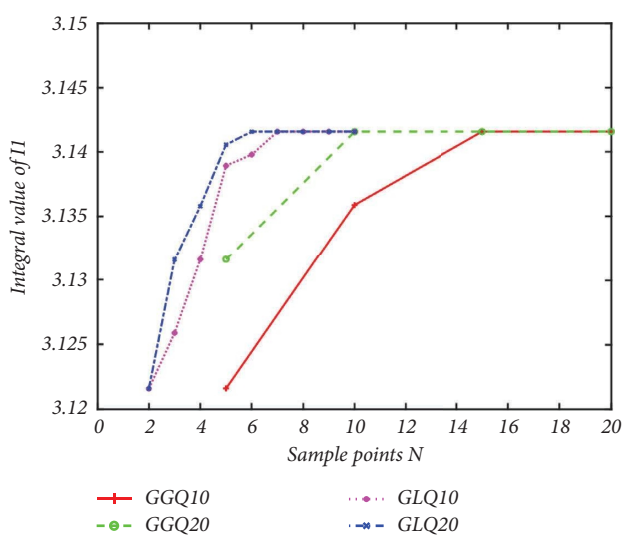

Figure 7: A comparison between the computed value GQH and the integral value of function $f=1$ over ellipsoid determined by GGQ.

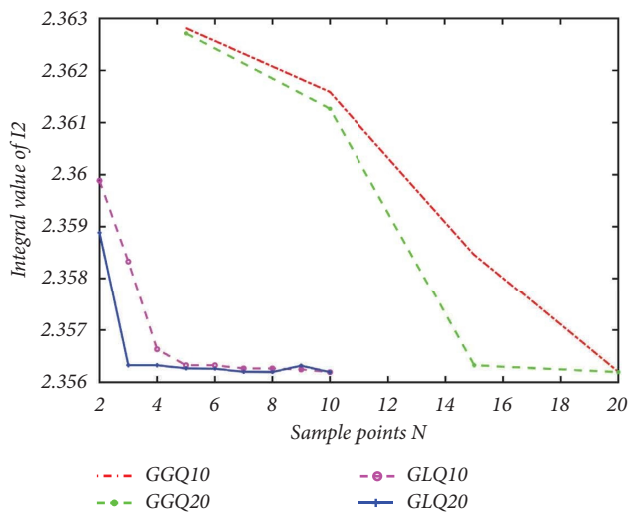

Figure 8: A comparison between the computed value GQH and the integral value of function $f = x^2 y$ over ellipsoid determined by GGQ.

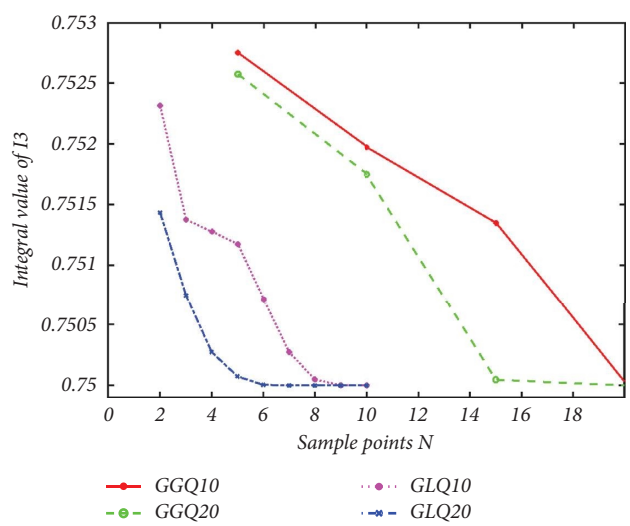

Figure 9: A comparison between the computed value GQH and the integral value of function $f = x^2 yz$ over ellipsoid determined by GGQ.

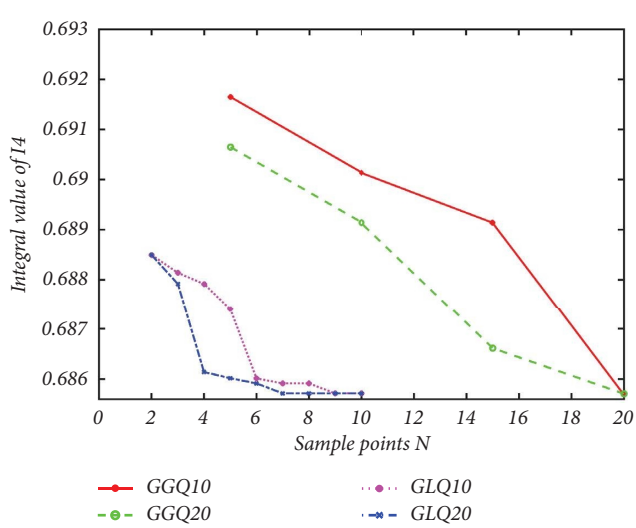

Figure 10: A comparison between the computed value GQH and the integral value of function $f = \sqrt{x + y + z}$ over ellipsoid determined by GGQ.

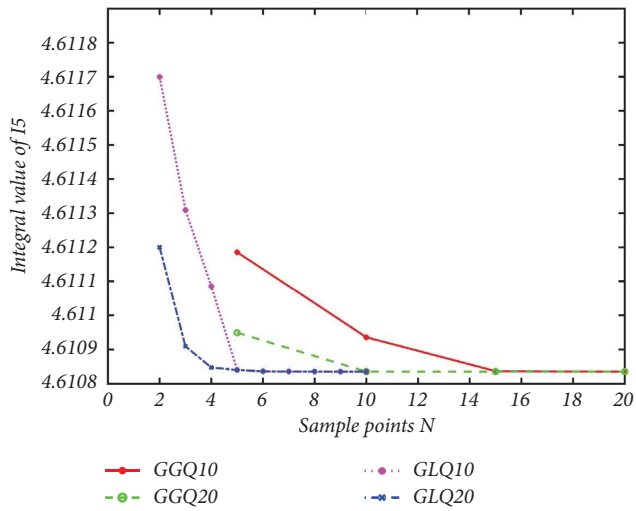

Figure 11: A comparison between the computed value GQH and the integral value of function $f = 1/\sqrt{x+y+z}$ over ellipsoid determined by GGQ.

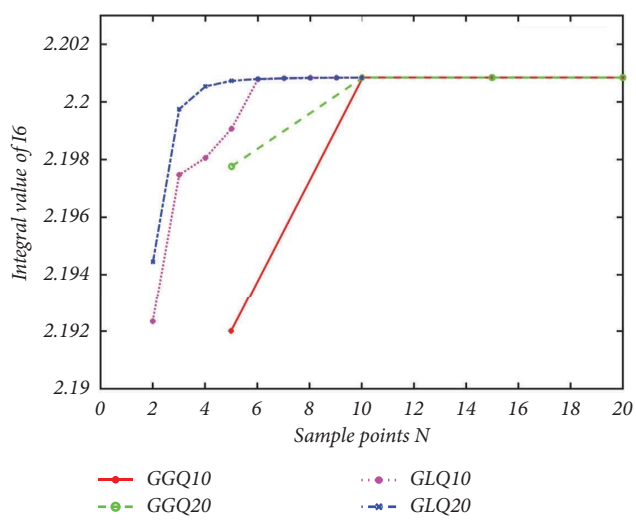

Figure 12: A comparison between the computed value GQH and the integral value of function $f = \mathrm{xyz}$ over ellipsoid determined by GGQ.

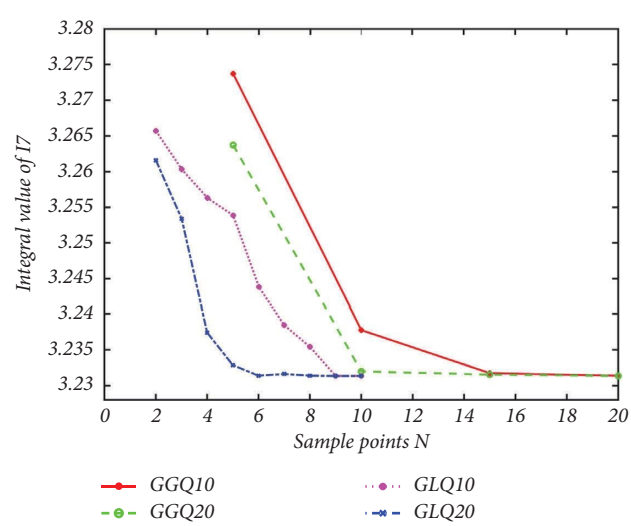

Figure 13: A comparison between the computed value GQH and the integral value of function $f = x^2 y^2$ over ellipsoid determined by GGQ.

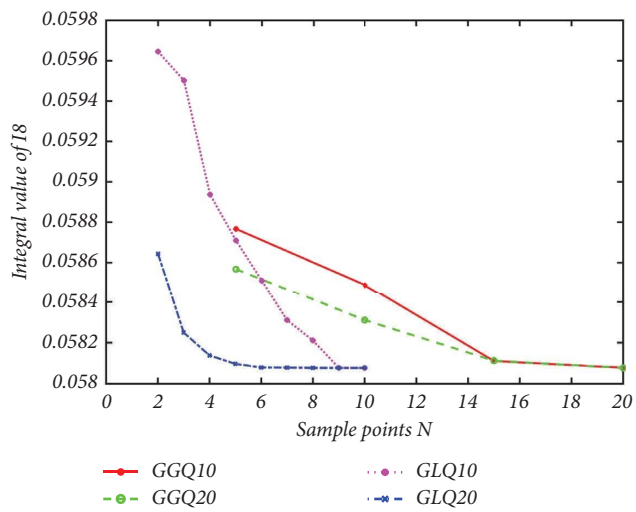

Figure 14: A comparison between the computed value GQH and the integral value of function $f = (1 + x + y + z)^{-4}$ over ellipsoid determined by GGQ.

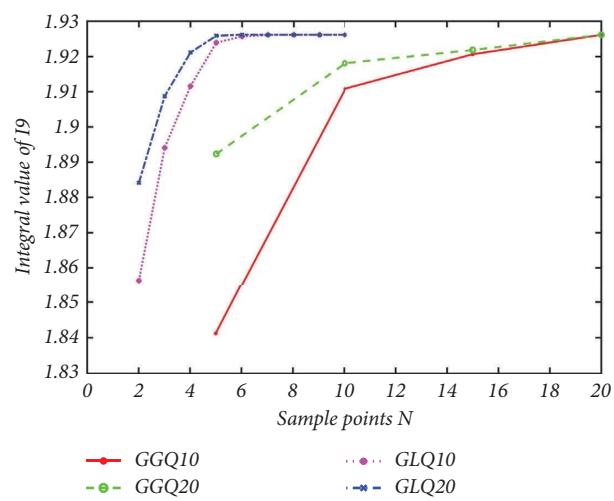

Figure 15: A comparison between the computed value GQH and the integral value of function $f = \sin(x + y^2 + z^4)$ over ellipsoid determined by GGQ.

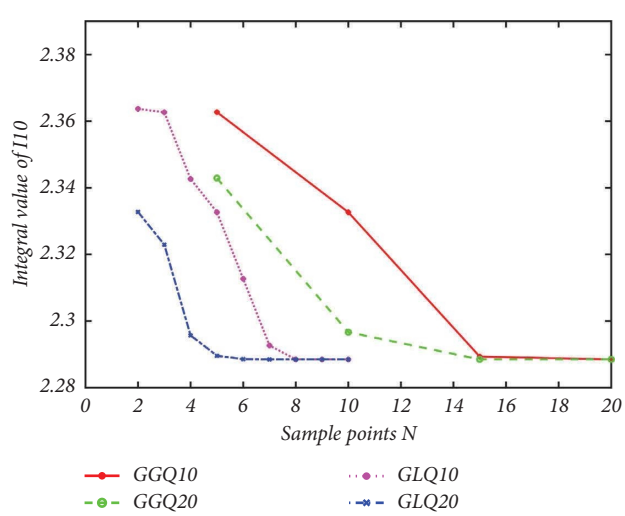

Figure 16: A comparison between the computed value GQH and the integral value of function $f = \sin(x^2 + y^2 + z^2)$ over ellipsoid determined by GGQ.

Table 7: Gaussian quadrature points for ellipse to 10-noded tetrahedron (transformed into hexahedron).

u	v	w	w_1
0.2279	0.2279	0.2279	0.0022
0.2738	0.2738	0.0611	0.0036
0.2738	0.0611	0.2738	0.0036
0.0611	0.2738	0.2738	0.0036
0.3417	0.07338	0.0734	0.0062
0.0734	0.3417	0.0734	0.0062
0.0734	0.0734	0.3417	0.0062
0.0916	0.0916	0.0916	0.0010
0.3163	0.2279	0.2279	0.0022
0.3912	0.2738	0.0611	0.0036
0.3912	0.2738	0.2738	0.0036
0.3912	0.0611	0.2738	0.0036
0.5115	0.3417	0.0734	0.0062
0.5115	0.0734	0.0734	0.0062
0.5115	0.0734	0.3417	0.0062
0.7253	0.0916	0.0916	0.0010
0.2279	0.3163	0.2279	0.0022
0.2738	0.3912	0.0610	0.0036
0.0610	0.3912	0.2738	0.0036
0.2738	0.3912	0.2738	0.0036
0.0734	0.5115	0.0734	0.0062
0.3417	0.5115	0.0734	0.0062
0.0734	0.5115	0.3417	0.0062
0.0916	0.7253	0.0916	0.0010
0.2279	0.2279	0.3163	0.0022
0.2738	0.2738	0.3912	0.0036
0.0611	0.2738	0.3912	0.0036
0.2738	0.0611	0.3912	0.0036
0.0734	0.3417	0.5115	0.0062
0.3417	0.0734	0.5115	0.0062
0.0734	0.0734	0.5115	0.0062
0.0916	0.0916	0.7253	0.0010

4.1. MATLAB Programme for Computing Integrals over Six Tetrahedral in First Octant of the Sphere. In this section, the implementation of the MATLAB code has been explained and provided in a supplementary document for Volume S1–S6, and the numerical integration of the example problems is considered to validate the quadrature method applied. The Gauss quadrature points and weights are given by the variables u, v, w, and w_1, respectively. The transformations derived are described by the variables x, y, z, and Jacobian J_1. The sample functions are represented as $f_1, f_2, \ldots, f_{10}$ for integration using the derived transformations. The code is run for each volume of tetrahedron, and the integral values are summed up for the six tetrahedral divisions in the first octant of the sphere.

Table 7 provides a succinct report that lists the Gaussian quadrature points of the ellipse to 10-noded tetrahedron (six tetrahedron in the first octant) and then turned into hexahedron.

5. Conclusions

In this paper, we derived transformations to compute the integrals numerically over the ellipsoid by dividing the ellipsoid into tetrahedral elements (quadratic and cubic) and, then, further discretizing the tetrahedral elements into hexahedral elements. An arbitrary ellipsoid is converted into a unit sphere by selecting a point P upon the sphere's surface (first octant) and discretized into 6 tetrahedral elements (one curved face). Each curved tetrahedral element (quadratic and cubic) is transformed into a standard tetrahedron (10-noded) with straight sides. The six standard tetrahedron elements are further discretized into four hexahedral elements by using transformations as in [17]. The transformations derived in this paper, with the aspect of the created meshes over ellipsoid, are evaluated over certain sample integrands with rational functions and singular functions. By applying the derived transformations, we compute the triple-integral values of some integrands numerically over the ellipsoid. It is observed that the integral results obtained by using Gaussian quadrature rules, as in [17], are better compared to generalized Gaussian quadrature rules. The integral values converging to the exact values are also noticed, and thus, the processing time is reduced. The proposed method solves the integrals over the ellipsoid of integrands with singular functions. Curved tetrahedral elements can fit into any of the complicated boundaries of partial differential equations and integral over linear hexahedral elements require minimum evaluation time compared to quadratic and cubic tetrahedral elements. We propose the curved tetrahedral elements transformed into

linear hexahedral elements for numerical integral computation. The application of the proposed method to solve partial differential equations is the future scope of the work.

6. Scope of the Work

Future potentials are in abundance in the ever-evolving field of biomass and biorefinery. The potential of biomass and biorefineries as renewable energy sources that could displace fossil fuels, which in other words is biomass, has been studied in this research. Various energy outputs, including biofuels and biogas, can be analyzed properly through this study. As the globe moves towards sustainable energy sources, the demand for biomass-based energy products is anticipated to rise and is also capable of producing a variety of chemicals and materials, such as bioplastics, solvents based on biomass, and adhesives based on biomass. As biorefineries have a smaller carbon footprint compared to their conventional counterparts, they can be used in various applications such as packaging, building, and textiles. Alongside the precise solution and using the finite element methodology, this type of biorefinery can be solved. As a major application, biorefineries can assist with waste management by turning organic waste into beneficial products.

Data Availability

Data are available upon request.

Ethical Approval

This article does not contain any studies involving animal or human participants performed by any of the authors.

Conflicts of Interest

The authors declare that they have no conflicts of interest.

Authors' Contributions

T.M. Mamatha investigated the study, developed the methodology, and wrote the original draft. B. Venkatesh* and P. Senthil Kumar* conceptualized the study, validated the study, and supervised the study. S. Mullai Venthan, M.S. Nisha, and Gayathri Rangasamy provided formal analysis, curated data, and validated the study.

Supplementary Materials

The MATLAB code is given in supplementary file as Volume S1–S6. (*Supplementary Materials*)

References

[1] P. C. Hammer and A. H. Stroud, "Numerical evaluation of multiple integrals. II," *Mathematics of Computation*, vol. 12, no. 64, pp. 272–280, 1958.

[2] P. C. Hammer and A. H. Stroud, "Numerical integration over simplexes," *Mathematical Tables and Other Aids to Computation*, vol. 10, no. 55, pp. 137–139, 1956.

[3] H. T. Rathod, H. S. G. Rao, and S. V. Hiremath, "Symbolic integration of polynomial functions over a linear polyhedron in Euclidean three-dimensional space," *Communications in Numerical Methods in Engineering*, vol. 12, no. 8, pp. 461–470, 1996.

[4] H. T. Rathod and B. Venkatesh, "Gauss Legendre-Gauss Jacobi quadrature rules over a Tetrahedral region," *International Journal of Mathematical Analysis*, vol. 5, no. 1–4, pp. 189–198, 2011.

[5] L. R. M. Maas, "On the surface area of an ellipsoid and related integrals of elliptic integrals," *Journal of Computational and Applied Mathematics*, vol. 51, no. 2, pp. 237–249, 1994.

[6] R. A. Krajcik and K. D. McLenithan, "Integrals and series related to the surface area of arbitrary ellipsoids," 2006, https://arxiv.org/ftp/math/papers/0605/0605216.pdf.

[7] L. E. Sjöberg and M. Shirazian, "Solving the direct and inverse geodetic problems on the ellipsoid by numerical integration," *Journal of Surveying EngineeringJournal of Surveying Engineering*, vol. 138, no. 1, pp. 9–16, 2012.

[8] J. Ma, V. Rokhlin, and S. Wandzura, "Generalized Gaussian quadrature rules for systems of arbitrary functions," *SIAM Journal on Numerical Analysis*, vol. 33, no. 3, pp. 971–996, 1996.

[9] K. T. Shivaram, "Generalised Gaussian quadrature over a sphere," *American Journal of Engineering Research and Reviews*, vol. 2, no. 9, pp. 290–293, 2013.

[10] M. Zlámal, "Curved elements in the finite element method. I," *SIAM Journal on Numerical Analysis*, vol. 10, no. 1, pp. 229–240le, 1973.

[11] M. Zlámal, "The finite element method in domains with curved boundaries," *International Journal for Numerical Methods in Engineering*, vol. 5, no. 3, pp. 367–373, 1973.

[12] R. Scott, "Finite Element Techniques for Curved Boundaries," Thesis, MIT Library, Cambridge, MA, USA, 1973.

[13] E. L. Wachspress, "Rational basis functions," *State-of-the-art Survey of Finite Element Method*, pp. 235–239, 1981.

[14] W. Gordon and C. Hall, "Construction of curvilinear coordinate systems and applications to mesh generation," *International Journal for Numerical Methods in Engineering*, vol. 7, no. 4, pp. 461–477, 1973.

[15] W. Gordon and C. Hall, "Transfinite element methods: blending-function interpolation over arbitrary curved element domains," *Numerische Mathematik*, vol. 21, no. 2, pp. 109–129, 1973.

[16] T. M. Mamatha and B. Venkatesh, "Gauss quadrature rules for numerical integration over a standard tetrahedral element by decomposing into hexahedral elements," *Applied Mathematics and Computation*, vol. 271, pp. 1062–1070, 2015.

[17] T. M. Mamatha and B. Venkatesh, "Generalised Gaussian Quadrature rules for numerical integration over tetrahedral element," in *Proceedings of the 1st International conference on research in Engineering, Computers and Technology (ICRECT 2016)*, pp. 172–177, Surabaya, Indonesia, September 2016.

[18] T. M. Mamatha, B. Venkatesh, and R. Pramod, "Numerical integration over ellipsoid by transforming into 10-noded tetrahedral elements," *IOP Conference Series: Materials Science and Engineering*, vol. 310, no. 1, Article ID 012144, 2018.

[19] F. Zhou, X. Xu, and X. Zhang, "Numerical integration method for triple integrals using the second kind Chebyshev wavelets and Gauss–Legendre quadrature," *Computational and Applied Mathematics*, vol. 37, no. 3, pp. 3027–3052, 2018.

[20] J. Jaskowiec and N. Sukumar, "High-order cubature rules for tetrahedra," *International Journal for Numerical Methods in Engineering*, vol. 121, no. 11, pp. 2418–2436, 2020.

[21] T. Cui, W. Leng, H. Liu, L. Zhang, and W. Zheng, "High-order numerical quadratures in a tetrahedron with an implicitly defined curved interface," *ACM Transactions on Mathematical Software*, vol. 46, no. 1, p. 18, 2020.

[22] S. Marc Durufl´e, P. Grob, and P. Joly, "Influence of Gauss and Gauss-Lobatto quadrature rules on the accuracy of a quadrilateral finite element method in the time domain," *Numerical Methods for Partial Differential Equations*, vol. 25, no. 3, 2009.

[23] P. Suvarnakuta, S. Devahastin, and A. S. Mujumdar, "A mathematical model for low-pressure superheated steam drying of a biomaterial," *Chemical Engineering and Processing: Process Intensification*, vol. 46, no. 7, pp. 675–683, 2007.

[24] S. N. Rothstein, W. J. Federspiel, and S. R. Little, "A unified mathematical model for the prediction of controlled release from surface and bulk eroding polymer matrices," *Biomaterials*, vol. 30, no. 8, pp. 1657–1664, 2009.

[25] M. A. Zhuravkov and N. S. Romanova, "Determination of physical and mechanical properties of biomaterials on base of the nanoindentation technologies and fractional order models," *Russian Journal of Biomechanics*, vol. 20, pp. 5–22, 2016.

[26] R. Hedayati, M. Sadighi, M. Mohammadi-Aghdam, and A. A. &Zadpoor, "Analytical relationships for the mechanical properties of additively manufactured porous biomaterials based on octahedral unit cells," *Applied Mathematical Modelling*, vol. 46, pp. 408–422, 2017.

[27] Y. Sokolovskyy, M. Levkovych, O. Mokrytska, S. Yatsyshyn, Y. Kaspryshyn, and C. Strauss, "Mathematical models and analysis of deformation processes in biomaterials with fractal structure," 2019, https://ceur-ws.org/Vol-2488/paper11.pdf.

[28] M. Barzegari, D. Mei, S. V. Lamaka, and L. Geris, "Computational modeling of degradation process of biodegradable magnesium biomaterials," *Corrosion Science*, vol. 190, 2021.